Concentration dependent properties lead to plastic ratcheting in thin island electrodes on substrate under cyclic charging and discharging

Kai Guo [1], Wei Zhang [1], Brian W. Sheldon [1], Huajian Gao [1,*]

[1] School of Engineering, Brown University, Providence, RI 02912, USA.

* Corresponding author, Huajian Gao.

Telephone: 1-401-8632626

Fax: 1-401-8639025

Address: 184 Hope Street, Providence, RI 02912, USA

Email: huajian_gao@brown.edu

Abstract

It is known that the mechanical properties of electrodes in lithium-ion batteries, such as modulus, yield stress, and interfacial strength, can depend strongly on lithium concentration. Here we show that a thin film island electrode with properties dependent on lithium concentration naturally undergoes plastic ratcheting with accumulative deformation and failure during cyclic charging and discharging. Some key predictions from numerical simulations are validated by galvanostatic tests. Strategies to avoid ratcheting include limiting the electrode size and/or selecting a balanced combination of concentration dependent materials properties.

Keywords: lithium-ion batteries; electrodes; concentration dependent materials properties; ratcheting; failure

1. Introduction

Lithium-ion batteries (LIB) have attracted worldwide attention due to their high energy density and broad range of applications [1-4]. One of the most prominent high energy density anode materials is silicon (Si), with a theoretical specific capacity (4200 mAh g^{-1}) that far exceeds the graphite (372 mAh g^{-1}) used in most commercial cells [2, 3]. However, Si undergoes large volume changes (up to 300%) during lithiation (lithium insertion) and delithiation (lithium extraction), resulting in mechanical degradation of Si electrodes and poor cycling performance [5]. Lithiation/delithiation can induce surface cracking in Si thin films and nanoparticles even during the first cycle [5-13]. The newly exposed crack surfaces lead to irreversible lithium (Li) consumption and capacity loss in the forming/re-forming of solid electrolyte interphase (SEI) [14], and thus cyclic lithiation/delithiation is commonly accompanied by capacity fading [15, 16]. Experiments have provided direct observations of accumulative mechanical damage in the electrodes during cycling. Maranchi et al. [6] showed that fractured Si thin films develop into islands with substantially larger gaps after 30 lithiation/delithiation cycles. Kumar et al. [17] presented AFM images showing that cracks in SEI layers on Si electrodes grow wider and deeper with cycling. Such accumulative deformation in electrodes can be related to a phenomenon called plastic ratcheting found in a variety of systems under cyclic thermal/mechanical loadings, such as pressure vessels [18], fiber-reinforced composites [19], thin multilayers on substrate [20], interconnect structures [21] and thermal barriers [22-24]. Effective control/prevention of ratcheting is often crucial for

maintaining the cyclic stability of materials and structures [25].

A prerequisite to ratcheting is plastic yielding of materials under cyclic loadings, and lithiation and delithiation of Si is known to be associated with extensive plastic flow [26-29]. Therefore, it is important to explore the relationship between plastic flow and ratcheting in Si as well as other electrode materials. Thin films on metallic current collectors provide a well-defined configuration for fundamental investigations of lithiation-induced ratcheting. Haftbaradaran and Gao [30] demonstrated that a Si island on substrate undergoes ratcheting if the yield stress of Si and/or the interfacial sliding strength between Si and substrate take on different values during lithiation and delithiation. Brassart et al. [31] found that when the yield stress is low and charging rate is high, a spherical electrode experiences cyclic plasticity, which means after each cycle (excluding the first one) the electrode deforms back to its shape at the beginning of the cycle even though plastic deformation has occurred. Thus, an electrode with constant material properties during cycling does not automatically result in ratcheting. Jia and Li [32] investigated the failure mechanisms associated with wrinkling of a thin film electrode on a compliant substrate and revealed ratcheting induced necking and cracking at wrinkling troughs. Recently, Liu et al. [33] reported that wrinkling of a thin film coating on an electrode under cyclic plastic deformation induced by lithiation and delithiation could lead to ratcheting in the form of a growing wrinkling amplitude with cycling. An important factor that has been missing in these studies is that the material properties of lithiated Si, such as Young's modulus [34], yield stress [27, 29], interfacial strength [35], are highly dependent on the Li concentration and

should vary continuously during the charging/discharging cycles. Here, building on the above existing studies, we will show that plastic deformation in electrodes with concentration dependent materials properties naturally leads to ratcheting during lithiation/delithiation.

2. Ratcheting of a circular thin film island electrode with concentration dependent materials properties

To study ratcheting in electrodes with concentration dependent materials properties, we revisit the problem of a thin film island electrode adhering and sliding on a substrate [30, 36, 37]. The electrode material is modeled as elastic and perfectly plastic with yield stress σ_y. Take an unlithiated and stress-free electrode as the reference state. During cyclic lithiation and delithiation, the electrode is subject to a compositional strain of,

$$\varepsilon^c = \beta c, \tag{1}$$

where $\beta = \overline{\Omega}/3$ and $\overline{\Omega}$ is a dimensionless coefficient equal to the partial molar volume of Li times the molar concentration of Li in the fully lithiated electrode; c denotes the normalized Li concentration, with $c = 0$ corresponding to the unlithiated and $c = 1$ the fully lithiated state. For simplicity, we assume that c increases (decreases) linearly with respect to time during lithiation (delithiation) and that the island is so thin that Li concentration remains uniform in the island. The electrode slides on the substrate following a rigid-perfectly plastic law, i.e. the interface remains bonded wherever the interfacial shear stress τ is below the interfacial sliding

strength τ_0, but undergoes free sliding once $\tau = \tau_0$. We note that delamination between the electrode and substrate is also a crucial failure mechanism that requires a separate analysis in a future study. From a conservative point of view, we focus on the case that the electrode stays attached to the substrate in the presence of large interfacial sliding.

Figure 1a shows schematically a circular island electrode of thickness h and radius R on a rigid substrate. It is assumed that the island is sufficiently thin ($h << R$) that the normal stress components in the plane of the island are uniform along the thickness direction. During lithiation/delithiation cycles, if sliding occurs at all, it will take place in a "sliding zone" near the edge of the island, while near the center of the island, referred to as the "locked zone", remains bonded to the substrate in spite of the plastic deformation.

2.1 Ratcheting under concentration dependent interfacial sliding strength

Finite element simulations have been carried out for the model system of a circular amorphous silicon (a-Si) island electrode with thickness of 100 nm and radius of 7.5 μm on a rigid substrate. For simplicity, we first consider a case in which only the interfacial sliding strength τ_0 depends on the Li concentration, while the Young's modulus and yield stress remain constant during cycling. In light of previous *ab initio* molecular dynamics (AIMD) simulations [35] of the interfacial sliding strength between lithiated a-Si and Cu, we assume that τ_0 decreases linearly from $\tau_0^u = 100\,\mathrm{MPa}$ at the unlithiated state to $\tau_0^f = 40\,\mathrm{MPa}$ at the fully lithiated state

during lithiation and increases linearly from τ_0^f to τ_0^u during delithiation. The Young's modulus and yield stress of the Si electrode are taken to be 40 GPa and 1 GPa, respectively [27, 34]. The volume change of fully lithiated silicon is up to 300%. However, such a large deformation leads to plastic strain localization or cyclic plasticity in a few cycles, as well as some convergence issues when modeling the concentration dependent sliding strength, which dilutes our main focus on ratcheting-induced deformation and failure behaviors. To address these concerns, the dimensionless coefficient β is taken to be 10% and the state of charge parameter, c, is cycled from zero to 1. That is to say, a cyclic compositional strain of 10% is applied to the electrode, which is equivalent to a volume change of about 35%.

Figures 1b and 1c show the contour plots of the effective plastic strain and thickness change (μm) in the island after 15 cycles. The material within the locked zone at the center of the island undergoes extensive plastic deformation, while that in the sliding zone near the edge of the island slides freely along the radial direction. The radius change plotted in Fig. 1d shows that the island expands more during the lithiation half cycles than it shrinks during the delithiation half cycles, causing tensile ratcheting of the island in the form of an accumulative size increase each cycle. The net increase in size results in thinning of the island in the vicinity of the boundary between the locked and sliding zones as shown in Fig. 1c.

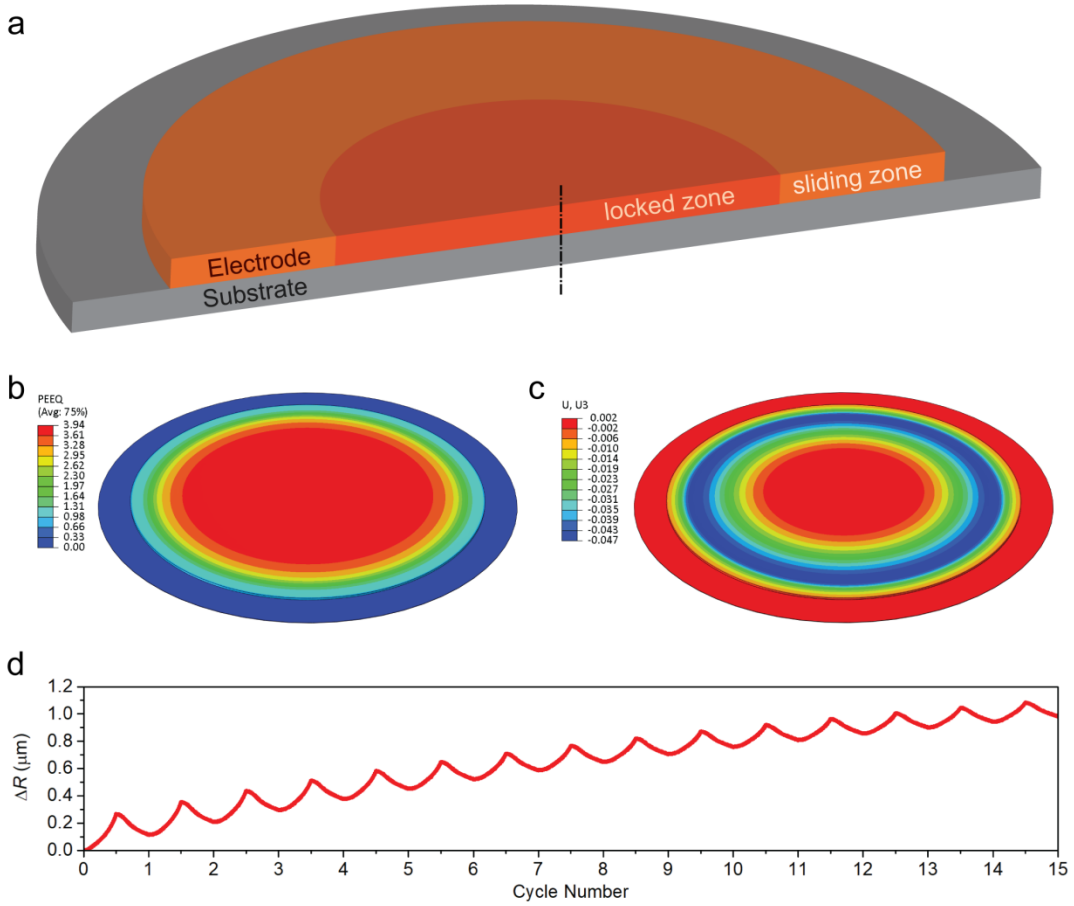

Figure 1. (a) Schematic of a circular thin island electrode on a substrate. Only one half of the structure is shown. (b-c) Contour plots of (b) the effective plastic strain and (c) thickness change (μm) in the circular island electrode with concentration dependent interfacial sliding strength ($\tau_0^u = 100\,\text{MPa}$ and $\tau_0^f = 40\,\text{MPa}$) after 15 cycles. (d) Evolution of the island radius during the first 15 cycles.

To demonstrate that ratcheting leads to failure, we take the interfacial sliding strengths at the unlithiated state and fully lithiated state as $\tau_0^u = 30\,\text{MPa}$ and $\tau_0^f = 20\,\text{MPa}$, respectively. Figure 2 shows that severe plastic strain localization has occurred in the island electrode, breaking the rotational symmetry of the problem. No instability occurs in the island after the first cycle. However, after 5 cycles, a wavy

pattern of the plastic strain appears in the vicinity of the boundary between the locked and sliding zones, developing into several plastic “channels” along the radial direction due to strain localization in the sliding zone. These “channels” develop into surface cracks as the thickness decreases after 10 cycles. Avoiding such ratcheting induced failure will be critical for structural integrity and electrochemical performance of any electrodes, as surface cracking could result in additional SEI formation on the newly exposed surfaces, leading to capacity degradation. It is worth pointing out that this failure mechanism is somewhat similar to that of a thin film electrode bonded to a compliant substrate [32], in which case plastic ratcheting is induced by film wrinkling, rather than by concentration dependent materials properties.

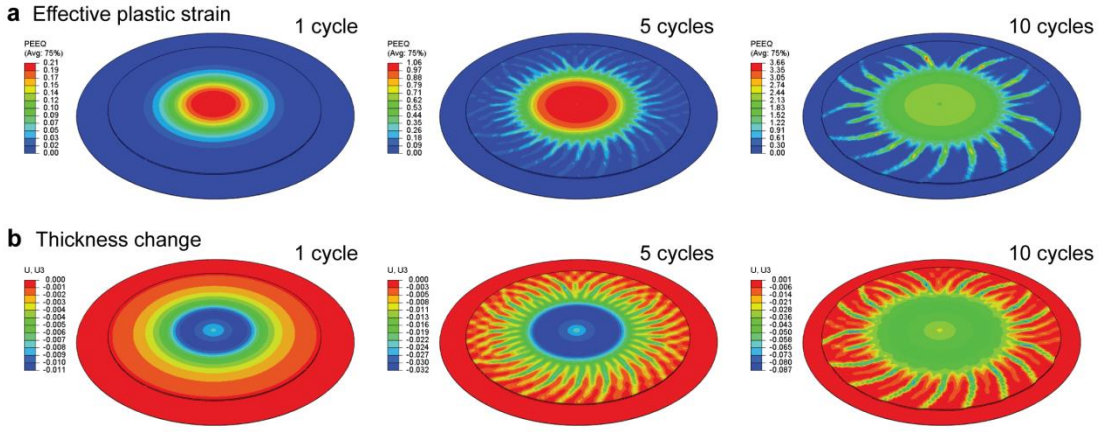

Figure 2. Contour plots of (a) the effective plastic strain and (b) thickness change (μm) in a circular island electrode with concentration dependent interfacial sliding strength ($\tau_0^u = 30\,\mathrm{MPa}$ and $\tau_0^f = 20\,\mathrm{MPa}$).

2.2 Ratcheting under concentration dependent yield stress

Next we consider 100 nm thick circular island electrodes with concentration

dependent yield stress σ_y and different radii. In this case, the Young's modulus and interfacial sliding strength are kept constant at 40 GPa and 40 MPa, respectively. The yield stress is taken to be $\sigma_y^u = 1.75\,\text{GPa}$ at the unlithiated state and $\sigma_y^f = 1\,\text{GPa}$ at the fully lithiated state according to *in situ* stress measurements [27]. We assume that σ_y decreases linearly from σ_y^u to σ_y^f during lithiation and increases linearly from σ_y^f to σ_y^u during delithiation. A compositional strain of 10% is applied to the electrode.

Figures 3a-d show contour plots of the effective plastic strain in the electrodes with different initial radii after 20 lithiation/delithiation cycles. For relatively small islands with initial radii of 5 μm and 7.5 μm, the locked zone where plastic deformation takes place remains circular (Figs. 3a and 3b), while instability was observed in a relatively large island with initial radius of 10 μm after 20 cycles (Fig. 3c), resulting in a wavy pattern of plastic strain near the boundary between the locked and sliding zones. As the initial radius increases to 15 μm, severe strain localization occurred, as shown in Fig. 3d, with drastic reduction in local thickness (Fig. 3e), forming surface cracks along the radial direction in the sliding zone. Figure 3f plots the radius changes of islands with different initial radii during the first 40 cycles. It can be seen that the islands with initial radii of 7.5 μm and 10 μm gradually shrink during the first several cycles, after which the shrinkage slows down, arriving at a state of cyclic plastic deformation with no net change in the island size, which is referred to as "plastic cycling" [18] or "cyclic plasticity" [31]. For the island with initial radius of 5 μm, cyclic plasticity occurred after the first lithiation half cycle.

However, the island with initial radius of 15 μm continues to shrink with strain localization. These results demonstrate that limiting electrode size is an effective strategy to avoid ratcheting as well as ratcheting-induced instabilities, which will be validated by galvanostatic tests in Section 2.4.

On a slightly different note, it has been reported that ratcheting can be induced in thermal barrier systems if all materials properties are temperature independent and including temperature dependent yielding would influence the ratcheting rate [24], which is analogous to what we discussed above regarding the concentration dependent yield stress. But, in our analysis, concentration dependent materials properties are the only mechanism inducing ratcheting, which provides further physical insights that we will discuss in Section 3.

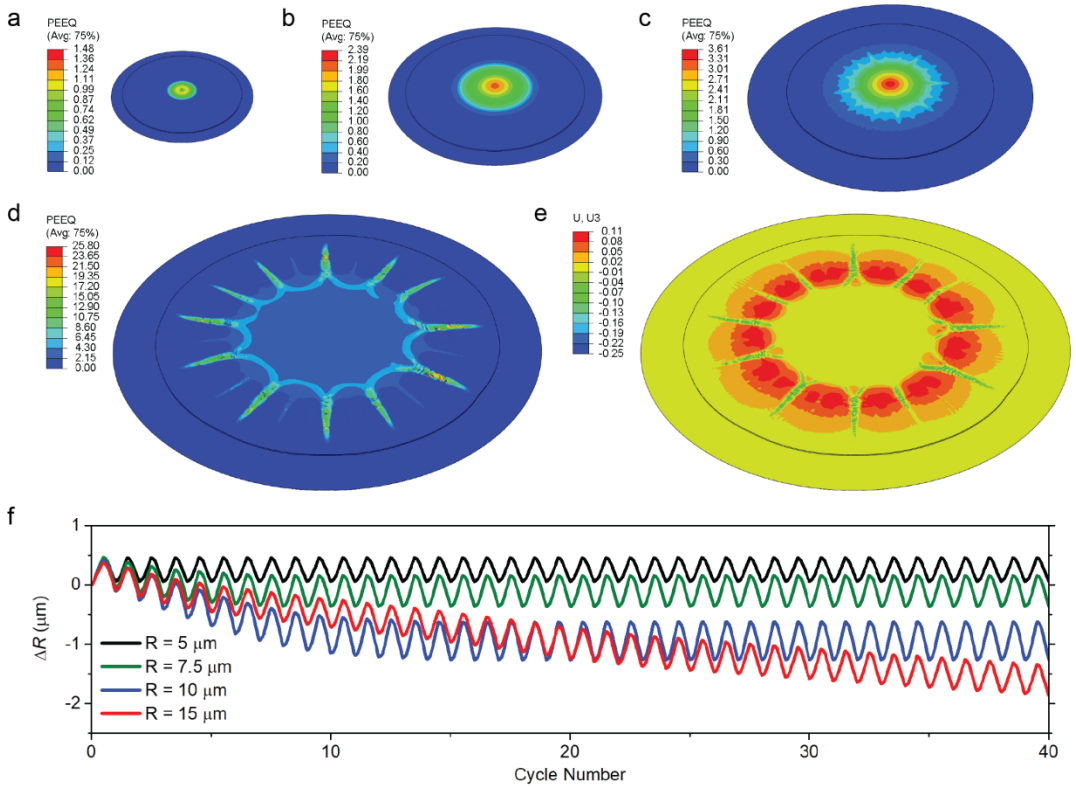

Figure 3. (a-d) Contour plots of the effective plastic strain in circular island

electrodes with concentration dependent yield stress and initial radius of (a) 5 μm; (b) 7.5 μm; (c) 10 μm; (d) 15 μm after 20 cycles. (e) Contour plot of the thickness change (μm) in a circular island electrode with concentration dependent yield stress and an initial radius of 15 μm after 20 cycles. (f) Radius changes of islands with different initial radii during the first 40 cycles.

In our finite element models, there is no initial surface perturbation to trigger the instabilities. Rather, the instability emerges during the finite element simulation runs. In order to demonstrate that the plastic strain localization shown in Figs. 2 and 3 are not numerical artefacts associated with the finite element mesh, we have implemented different meshing techniques and mesh sizes, and the results show that the patterns of plastic strain localization are similar for different meshes and the spacing between two adjacent surface cracks is independent of the mesh size. We speculate that the spacing between surface cracks is governed by the size and material properties of the island electrode. However, the aim of the present study is to elucidate the relationship between concentration dependent material properties and ratcheting. Developing a model to account for the intrinsic mechanisms of the ratcheting-induced instabilities and to predict the characteristic lengthscales will be left to a separate analysis in the future.

Moreover, it is worth pointing out that the surface cracking shown in Figs. 2 and 3 is different from the mudcracking that occurs during the first cycle in thin film electrodes. The latter is attributed to the tensile film stress during delithiation, while

the former is induced by ratcheting and plastic strain localization and thus occurs after a number of lithiation/delithiation cycles. We look forward to further experiments to evidence this failure mechanism.

2.3 Ratcheting under multiple concentration dependent materials properties

The analysis above shows that the concentration dependent interfacial sliding strength with τ_0^u higher than τ_0^f activates tensile ratcheting while the concentration dependent yield stress with σ_y^u higher than σ_y^f induces compressive ratcheting. Other concentration dependent materials properties, such as Young's modulus and thickness variation due to lithiation and delithiation, could also lead to ratcheting (see Figs. S1 and S2). In order to demonstrate whether tensile or compressive ratcheting would be induced when all materials properties become concentration dependent at the same time, we have performed finite element simulations of a circular a-Si island electrode with thickness of 100 nm and radius of 7.5 μm adhering and sliding on a substrate. We adopt the results from previous density functional theory (DFT) calculations that the Young's modulus of lithiated Si is about 90 GPa at the unlithiated and 34 GPa at the fully lithiated state [34]. Moreover, the yield stress varies linearly between 1.75 GPa at the unlithiated state and 1 GPa at the fully lithiated state during cycling [27]. The interfacial sliding strength at the fully lithiated state is set to $\tau_0^f = 40\,\text{MPa}$, but the sliding strength at the unlithiated state τ_0^u could not be determined since the AIMD calculations imply that τ_0^u can take on any value between 40 and 300 MPa depending on the amount of Li residue at the Si/substrate

interface after delithiation [35]. A compositional strain of 10% is applied.

Figure 4a shows the radius change of the island for different values of τ_0^u, and the ratcheting rate (i.e., the net radius change per each cycle) is plotted in Fig. 4b as a function of τ_0^u. It is seen that there exists a critical sliding strength at the unlithiated state $\tau_{0,c}^u$ such that the island incrementally expands (shrinks) per each cycle if τ_0^u is above (below) $\tau_{0,c}^u$. If τ_0^u is equal to $\tau_{0,c}^u$, cyclic plasticity would take place as the effects of various concentration dependent materials properties are counterbalanced. The analysis suggests that whether tensile or compressive ratcheting occurs can be influenced by the values of concentration dependent properties and there is another potential approach to prevent ratcheting by achieving a balanced combination of concentration dependent materials properties. It should be pointed out that the feasibility of this approach needs to be further studies as tweaking the composition of the electrode material during fabrication usually alters all materials properties at the same time.

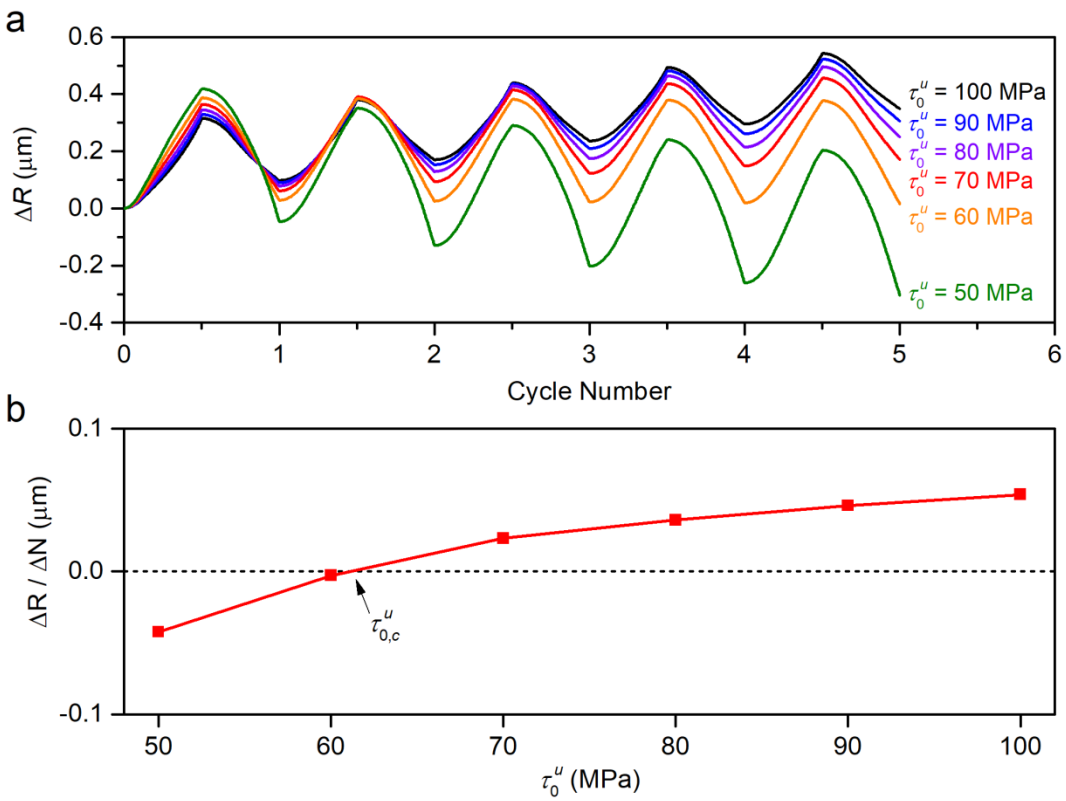

Figure 4. (a) Radius change of an island with various concentration dependent materials properties adopted from experimental measurements or DFT calculations, except for the interfacial sliding strength at the unlithiated state whose value is varied as a model parameter. (b) Ratcheting rate at the 5th cycle as a function of the interfacial sliding strength at the unlithiated state.

2.4 Galvanostatic tests on patterned circular Si islands

Our analysis above revealed that both tensile and compressive ratcheting could occur in a thin island electrode during cyclic charging/discharging, as long as the material properties, including Young's modulus, yield stress and interfacial sliding strength, are dependent on Li concentration. At this point, we do not have full knowledge of the concentration dependence of all material properties and it is

therefore difficult to fully validate the theoretical predictions with experiments. Nevertheless, it is still interesting to validate some of the key predictions from numerical simulations. For this purpose, galvanostatic discharge/charge tests were performed on patterned 100 nm thick circular Si islands (with initial radii of 5 μm and 10 μm) at the current density of C/5 for 1 and 10 cycles, respectively. After the galvanostatic tests, these patterned islands were examined with scanning electron microscopy (FIB, FEI HELIOS 600). Figures 5a and 5b show the SEM images of the islands before cycling, after the first cycle, and after the 10th cycle. The radii of the islands were measured and averaged through several randomly selected SEM images and the relative change in radius was plotted in Fig. 5c. During the first cycle, the island size increase is mainly ascribed to the irreversible volume change upon lithiation of pristine Si. Interestingly, it is found that the average size of the islands increases between the first cycle and the 10th cycle, indicating tensile ratcheting. This result is opposite to the compressive ratcheting observed in fractured Si thin films [6]. These experimental evidences support the prediction from our simulations that different values of concentration dependent properties due to different experimental setups could result in tensile as well as compressive ratcheting of island electrodes. In addition, Fig. 5c shows that the islands with initial radius of 5 μm have smaller relative change in radius compared to those with initial radius of 10 μm, which is consistent with the finite element results shown in Fig. 3f, evidencing the feasibility of the proposed approach to prevent ratcheting by limiting the electrode size.

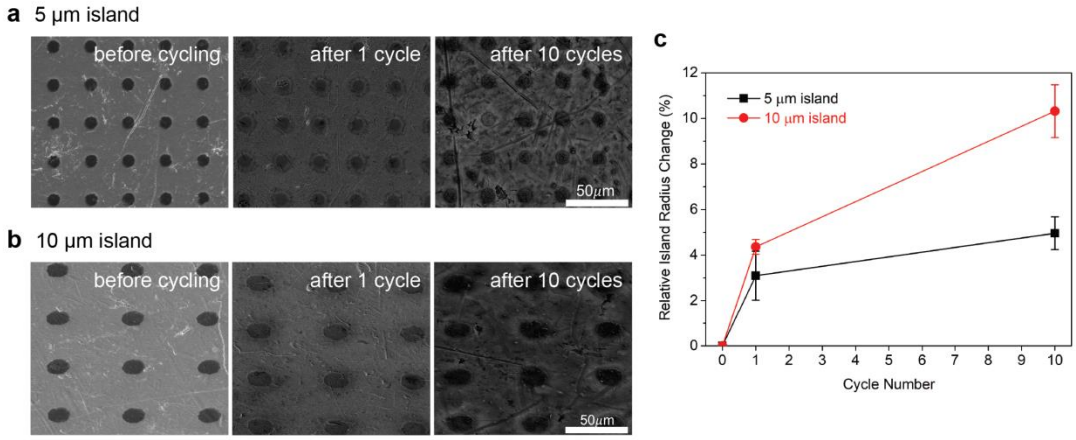

Figure 5. SEM images of patterned circular Si islands with initial radii of (a) 5 μm and (b) 10 μm. (c) Relative change in average radius of the islands.

3. Analytical model of ratcheting under concentration dependent materials properties

To understand and support the above simulation results, we constructed an analytical model for a plane stress thin island electrode with concentration dependent interfacial sliding strength adhering and sliding on a rigid substrate (see details in Appendix A). Previously, analytical solutions have been obtained for a plastically deforming plane stress thin film island electrode [30] and an elastic circular island electrode [36] under the condition that all material properties are constant. The concentration dependence of material properties introduces substantial complexity to such problems, and theoretical analysis of a plane strain or axisymmetric thin film island electrode seems too complicated to fit the scope of the present work. Therefore, we consider a plane stress analytical model, while overly simplistic in some aspects, nevertheless capable of capturing the essential mechanisms of ratcheting with

predictions in good agreement with numerical simulations (see Fig. A.4).

Define a dimensionless island half-length change as

$$\Delta\bar{L} = \frac{\Delta L}{\max\{|\Delta L_{\mathrm{li}}|, |\Delta L_{\mathrm{de}}|\}}, \tag{2}$$

where ΔL_{li} and ΔL_{de} are net changes in island half-length L during a lithiation half cycle and a delithiation half cycle, respectively. Figure 6 plots the variation of $\Delta\bar{L}$ during a full lithiation/delithiation cycle. The result suggests that the variation of $\Delta\bar{L}$ exhibits two distinct stages during each lithiation or delithiation half cycle: an "elastic stage" appears first as the entire island undergoes elastic deformation, followed by plastic yielding in the island, at which point the "elastic stage" ends and a "plastic stage" sets in and continues until the end of the half cycle. Note that the concentration dependent sliding strength τ_0 is symmetric during a full cycle, i.e., the value of τ_0 at a certain concentration during lithiation is equal to that at the same concentration during delithiation (see the green line in Fig. 6). However, the island length change is asymmetric owing to two intrinsic mechanisms associated with this two-stage deformation mode: (i) the averaged value of τ_0 at the elastic (plastic) stage during lithiation is higher (lower) than that at the elastic (plastic) stage during delithiation (see the dashed and solid parts of the green line in Fig. 6); (ii) the ratio of the elastic stage in a lithiation half cycle is slightly different from that in a delithiation half cycle. These two mechanisms result in symmetry breaking of the problem, with different island length change during lithiation and delithiation half cycles, leading to ratcheting.

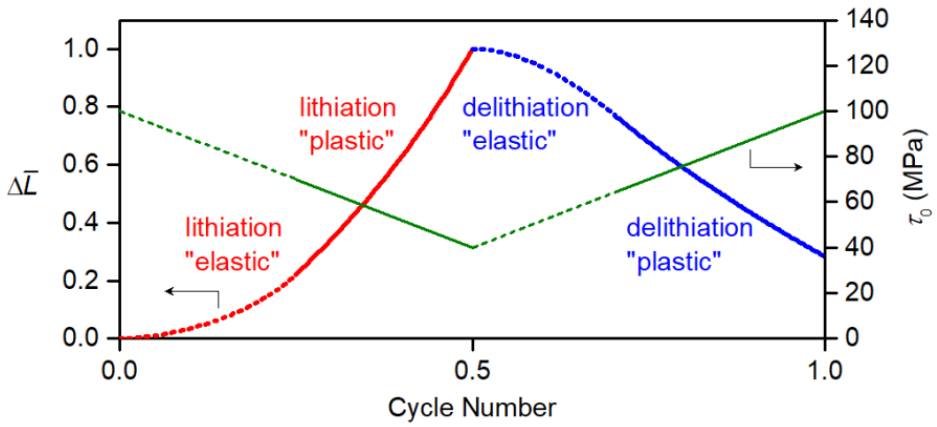

Figure 6. Theoretical prediction of the dimensionless half-length change of a plane stress island electrode with concentration dependent interfacial sliding strength ($\tau_0^u = 100\,\text{MPa}$ and $\tau_0^f = 40\,\text{MPa}$). The thickness, Young's modulus and yield stress of the electrode are selected to be 100 nm, 40 GPa and 1 GPa, respectively.

The two mechanisms that triggered the symmetry breaking of island deformation suggest two ways to restrain ratcheting. The first is to minimize or maximize the ratios of the elastic stages in lithiation and delithiation half cycles by decreasing or increasing the critical concentration,

$$c^e = \frac{2\sigma_y}{E\beta}. \tag{3}$$

If τ_0^u is greater than τ_0^f, c^e denotes the ratio of the elastic stage in a lithiation half cycle, and the ratio of the elastic stage in a delithiation half cycle is less than c^e. The dimensionless ratcheting rate as a function of c^e is plotted in Fig. 7a. As c^e approaches zero, the ratcheting rate also goes to zero since the island undergoes plastic deformation during the entire cycle and thus the symmetry breaking effect associated with two stage deformation ceases to exist, leading to cyclic plasticity. If

c^e approaches one, although the island undergoes purely elastic deformation during lithiation, plastic deformation occurs at the boundary between the locked and sliding zones during delithiation, leading to a positive ratcheting rate. By further increasing c^e, the island eventually avoids plastic yielding during delithiation, and the ratcheting rate decreases to zero. A maximum ratcheting rate is reached at a finite value of c^e.

Figure 7b shows the dimensionless ratcheting rate $\Delta\bar{L}/\Delta N$ as a function of $\Delta\tau_0 = \tau_0^u - \tau_0^f$ with average sliding strength $\tau_{0,\text{avg}} = (\tau_0^u + \tau_0^f)/2$ fixed. It is seen that $\Delta\bar{L}/\Delta N$ is an antisymmetric function of $\Delta\tau_0$, as predicted by our analytical model. Tensile ratcheting takes place if τ_0^u is greater than τ_0^f and compressive ratcheting occurs if τ_0^u is less than τ_0^f. In addition, the magnitude of the ratcheting rate increases with increasing $|\Delta\tau_0| = |\tau_0^u - \tau_0^f|$. This suggests that another way to suppress ratcheting is by reducing the concentration dependency of τ_0. Figure 7 shows that the predictions of our plane stress analytical model discussed above are in good agreement with finite element simulations. Here the analytical model is limited to concentration dependent interfacial sliding strength only. In practice, the electrode has multiple material properties depending on Li concentration, and it is at least theoretically possible to avoid ratcheting by designing a balanced combination of concentration dependent materials properties, as discussed in Section 2.3.

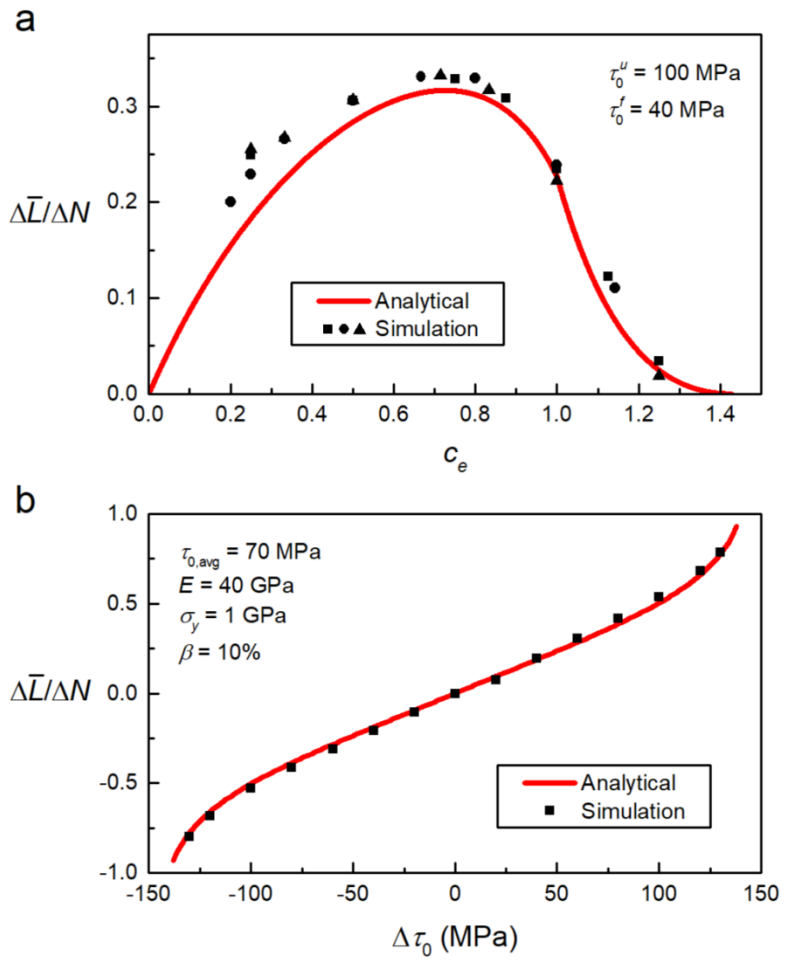

Figure 7. Dimensionless ratcheting rate $\Delta\bar{L}/\Delta N$ as a function of (a) c^e and (b) $\Delta\tau_0 = \tau_0^u - \tau_0^f$ for a 100 nm plane stress thin island electrode with concentration dependent interfacial sliding strength. The average sliding strength $\tau_{0,\text{avg}} = (\tau_0^u + \tau_0^f)/2 = 70\,\text{MPa}$ is fixed. The square dots in (a) are simulation results with varing σ_y, $E = 40\,\text{GPa}$ and $\beta = 10\%$; The round dots are simulation results with varing E, $\sigma_y = 1\,\text{GPa}$ and $\beta = 10\%$; The triangular dots are simulation results with varing β, $E = 40\,\text{GPa}$ and $\sigma_y = 1\,\text{GPa}$.

4. Conclusion

We have performed theoretical analysis and numerical simulations to investigate

ratcheting related failure in a thin film island electrode adhering and sliding on a substrate under cyclic charging and discharging. Given that the mechanical properties of electrode materials, including modulus, yield stress, and interfacial strength, can strongly depend on Li concentration, our analysis shows that plastic deformation in an electrode could naturally lead to ratcheting which in turns results in accumulative deformation during cycling. If ratcheting occurs, even a small net change in size of the electrode per cycle could cause severe plastic strain localization and mechanical failure after a number of cycles, which would then lead to rapid capacity fading. Our analysis reveals there are potentially two strategies to avoid ratcheting instabilities. One is to limit the electrode size and the other is to achieve a balanced combination of concentration dependent materials properties. This work shows that mechanical degradation in the form of plastic ratcheting could be a universal phenomenon in electrochemical material systems subject to cycling, and the developed analytical model provides a guideline for the design of high capacity electrodes with improved cycle life in next generation lithium-ion batteries.

Modeling and experimental methods

Modeling. Finite element simulations were performed using the commercial software ABAQUS (Dassault Systemes Simulia Corp., Providence, RI). The lithiation-induced compositional strain is implemented through a thermal strain analogy. An ABAQUS user subroutine FRIC was used to model a rigid-perfectly plastic law of interfacial sliding with a “stiff elastic behavior” as shown in Fig. S3.

The interfacial sliding strength τ_0 is assumed to be independent of the contact pressure and total slip between the island electrode and substrate, but it could be a function of Li concentration. A small amount of elastic slip u_0 is permitted for $\tau \le \tau_0$, which is set to 0.5% of a "characteristic contact surface face dimension" in ABAQUS. Once τ_0 is reached, the electrode slides on the substrate with a constant sliding stress $\tau = \tau_0$.

Experiments. Thin film specimens were prepared by electron-beam evaporation at a rate of 1 Å/s. Typically, a 300 nm thick copper film used as the current collector was first deposited on steel disc substrate (0.5 mm thick, with diameter of 16 mm). Patterned silicon island was then deposited on top of the copper through custom brass masks (0.005 in. thick, with 10, or 20 μm holes separated by twice the hole spacing), and the thickness of the silicon film was 100 nm. Finally, the prepared films were placed in CR-2032 coin cells that were assembled in an Ar-filled glove box, where Li foil was both the counter and reference electrode. The electrolyte was a mixed solution of 1 M $LiPF_6$ in ethylene carbonate and ethylmethyl carbonate (3:7 volume ratio, Gotion, USA). Galvanostatic discharge/charge tests were performed with a Bio-Logic VSP potentiostat in a voltage window of 0.05-1.5 V (versus Li^+/Li) at a current density of C/5 for 1 and 10 cycles, respectively. After these tests, the coin cells were disassembled in the glove box and the silicon electrodes were examined with scanning electron microscopy (FIB, FEI HELIOS 600).

Acknowledgments

The authors acknowledge the support by the Assistant Secretary for Energy Efficiency and Renewable Energy, Vehicle Technologies Office of the U.S. Department of Energy under Contract No. Award Number DE-EE0007787 under the Battery Material Research (BMR) Program, as well as support from SK Innovation.

Declarations of interest: none

References

[1] J.M. Tarascon, M. Armand, Issues and challenges facing rechargeable lithium batteries, Nature 414 (2001) 359-367.
[2] U. Kasavajjula, C.S. Wang, A.J. Appleby, Nano- and bulk-silicon-based insertion anodes for lithium-ion secondary cells, J. Power Sources 163 (2007) 1003-1039.
[3] C.K. Chan, H.L. Peng, G. Liu, K. McIlwrath, X.F. Zhang, R.A. Huggins, Y. Cui, High-performance lithium battery anodes using silicon nanowires, Nat. Nanotechnol. 3 (2008) 31-35.
[4] M. Armand, J.M. Tarascon, Building better batteries, Nature 451 (2008) 652-657.
[5] L.Y. Beaulieu, K.W. Eberman, R.L. Turner, L.J. Krause, J.R. Dahn, Colossal reversible volume changes in lithium alloys, Electrochem. Solid-State Lett. 4 (2001) A137-A140.
[6] J.P. Maranchi, A.F. Hepp, A.G. Evans, N.T. Nuhfer, P.N. Kumta, Interfacial properties of the a-Si/Cu: active-inactive thin-film anode system for lithium-ion batteries, J. Electrochem. Soc. 153 (2006) A1246-A1253.
[7] J.C. Li, A.K. Dozier, Y.C. Li, F.Q. Yang, Y.T. Cheng, Crack Pattern Formation in Thin Film Lithium-Ion Battery Electrodes, J. Electrochem. Soc. 158 (2011) A689-A694.
[8] Y.H. Wang, Y. He, R.J. Xiao, H. Li, K.E. Aifantis, X.J. Huang, Investigation of crack patterns and cyclic performance of Ti-Si nanocomposite thin film anodes for lithium ion batteries, J. Power Sources 202 (2012) 236-245.
[9] X.H. Liu, L. Zhong, S. Huang, S.X. Mao, T. Zhu, J.Y. Huang, Size-Dependent Fracture of Silicon Nanoparticles During Lithiation, ACS Nano 6 (2012) 1522-1531.
[10] Y. He, X.Q. Yu, G. Li, R. Wang, H. Li, Y.L. Wang, H.J. Gao, X.J. Huang, Shape evolution of patterned amorphous and polycrystalline silicon microarray thin film electrodes caused by lithium insertion and extraction, J. Power Sources 216 (2012) 131-138.

[11] M.T. McDowell, I. Ryu, S.W. Lee, C.M. Wang, W.D. Nix, Y. Cui, Studying the Kinetics of Crystalline Silicon Nanoparticle Lithiation with In Situ Transmission Electron Microscopy, Adv. Mater. 24 (2012) 6034-6041.
[12] M. Pharr, Z.G. Suo, J.J. Vlassak, Measurements of the Fracture Energy of Lithiated Silicon Electrodes of Li-Ion Batteries, Nano Lett. 13 (2013) 5570-5577.
[13] L. Yang, H. Chen, H. Jiang, Y. Wei, W. Song, D. Fang, Failure mechanisms of 2D silicon film anodes: in situ observations and simulations on crack evolution, Chem. Commun. 54 (2018) 3997-4000.
[14] D. Aurbach, Review of selected electrode-solution interactions which determine the performance of Li and Li ion batteries, J. Power Sources 89 (2000) 206-218.
[15] T. Ohzuku, H. Tomura, K. Sawai, Monitoring of particle fracture by acoustic emission during charge and discharge of Li/MnO2 cells, J. Electrochem. Soc. 144 (1997) 3496-3500.
[16] H.F. Wang, Y.I. Jang, B.Y. Huang, D.R. Sadoway, Y.T. Chiang, TEM study of electrochemical cycling-induced damage and disorder in LiCoO2 cathodes for rechargeable lithium batteries, J. Electrochem. Soc. 146 (1999) 473-480.
[17] R. Kumar, A. Tokranov, B.W. Sheldon, X.C. Xiao, Z.Q. Huang, C.Z. Li, T. Mueller, In Situ and Operando Investigations of Failure Mechanisms of the Solid Electrolyte Interphase on Silicon Electrodes, ACS Energy Lett. 1 (2016) 689-697.
[18] J. Bree, Elastic-plastic behaviour of thin tubes subjected to internal pressure and intermittent high-heat fluxes with application to fast-nuclear-reactor fuel elements, J. Strain Anal. 2 (1967) 226-238.
[19] S. Jansson, F.A. Leckie, Mechanical-Behavior of a Continuous Fiber-Reinforced Aluminum Matrix Composite Subjected to Transverse and Thermal Loading, J. Mech. Phys. Solids 40 (1992) 593-612.
[20] M.R. Begley, A.G. Evans, Progressive cracking of a multilayer system upon thermal cycling, J. Appl. Mech. 68 (2001) 513-520.
[21] M. Huang, Z. Suo, Q. Ma, Plastic ratcheting induced cracks in thin film structures, J. Mech. Phys. Solids 50 (2002) 1079-1098.
[22] M.Y. He, A.G. Evans, J.W. Hutchinson, The ratcheting of compressed thermally grown thin films on ductile substrates, Acta Mater. 48 (2000) 2593-2601.
[23] D.R. Mumm, A.G. Evans, I.T. Spitsberg, Characterization of a cyclic displacement instability for a thermally grown oxide in a thermal barrier system, Acta Mater. 49 (2001) 2329-2340.
[24] A.M. Karlsson, G. Evans, A numerical model for the cyclic instability of thermally grown oxides in thermal barrier systems, Acta Mater. 49 (2001) 1793-1804.
[25] S. Suresh, Fatigue of Materials, second ed., Cambridge University Press, Cambridge, 1998.
[26] T. Takamura, S. Ohara, M. Uehara, J. Suzuki, K. Sekine, A vacuum deposited Si film having a Li extraction capacity over 2000 mAh/g with a long cycle life, J. Power Sources 129 (2004) 96-100.
[27] V.A. Sethuraman, M.J. Chon, M. Shimshak, V. Srinivasan, P.R. Guduru, In situ measurements of stress evolution in silicon thin films during electrochemical lithiation and delithiation, J. Power Sources 195 (2010) 5062-5066.

[28] K.J. Zhao, W.L. Wang, J. Gregoire, M. Pharr, Z.G. Suo, J.J. Vlassak, E. Kaxiras, Lithium-Assisted Plastic Deformation of Silicon Electrodes in Lithium-Ion Batteries: A First-Principles Theoretical Study, Nano Lett. 11 (2011) 2962-2967.
[29] K.J. Zhao, G.A. Tritsaris, M. Pharr, W.L. Wang, O. Okeke, Z.G. Suo, J.J. Vlassak, E. Kaxiras, Reactive Flow in Silicon Electrodes Assisted by the Insertion of Lithium, Nano Lett. 12 (2012) 4397-4403.
[30] H. Haftbaradaran, H.J. Gao, Ratcheting of silicon island electrodes on substrate due to cyclic intercalation, Appl. Phys. Lett. 100 (2012) 121907.
[31] L. Brassart, K.J. Zhao, Z.G. Suo, Cyclic plasticity and shakedown in high-capacity electrodes of lithium-ion batteries, Int. J. Solids Struct. 50 (2013) 1120-1129.
[32] Z. Jia, T. Li, Failure mechanics of a wrinkling thin film anode on a substrate under cyclic charging and discharging, Extreme Mech. Lett. 8 (2016) 273-282.
[33] Y. Liu, K. Guo, C. Wang, H. Gao, Wrinkling and ratcheting of a thin film on cyclically deforming plastic substrate: Mechanical instability of the solid-electrolyte interphase in Li-ion batteries, J. Mech. Phys. Solids, In press.
[34] V.B. Shenoy, P. Johari, Y. Qi, Elastic softening of amorphous and crystalline Li-Si Phases with increasing Li concentration: A first-principles study, J. Power Sources 195 (2010) 6825-6830.
[35] M.E. Stournara, X.C. Xiao, Y. Qi, P. Johari, P. Lu, B.W. Sheldon, H.J. Gao, V.B. Shenoy, Li Segregation Induces Structure and Strength Changes at the Amorphous Si/Cu Interface, Nano Lett. 13 (2013) 4759-4768.
[36] H. Haftbaradaran, S.K. Soni, B.W. Sheldon, X.C. Xiao, H.J. Gao, Modified Stoney Equation for Patterned Thin Film Electrodes on Substrates in the Presence of Interfacial Sliding, J. Appl. Mech. 79 (2012) 031018.
[37] X. Xiao, P. Liu, M.W. Verbrugge, H. Haftbaradaran, H. Gao, Improved cycling stability of silicon thin film electrodes through patterning for high energy density lithium batteries, J. Power Sources 196 (2011) 1409-1416.

Appendix A. Analytical model of a plane stress island electrode with concentration dependent interfacial sliding strength

As illustrated in Fig. A.1a, consider the plane stress (i.e., assuming the stress components perpendicular to the plane of Fig. A.1a are negligible) problem of a thin film island electrode of thickness h and length $2L$ adhering and sliding on a rigid substrate. Plastic yielding in the island occurs when

$$\sigma \geq \sigma_y, \tag{A.1}$$

where σ denotes the normal stress in the film and σ_y the yield stress.

Taking advantage of the symmetry of the problem, only half of the island needs to be considered. Figure A.1b shows the free-body diagram for the half island during lithiation. The length of the sliding zone is given by,

$$l_p = \frac{\sigma_y h}{\tau_0}. \tag{A.2}$$

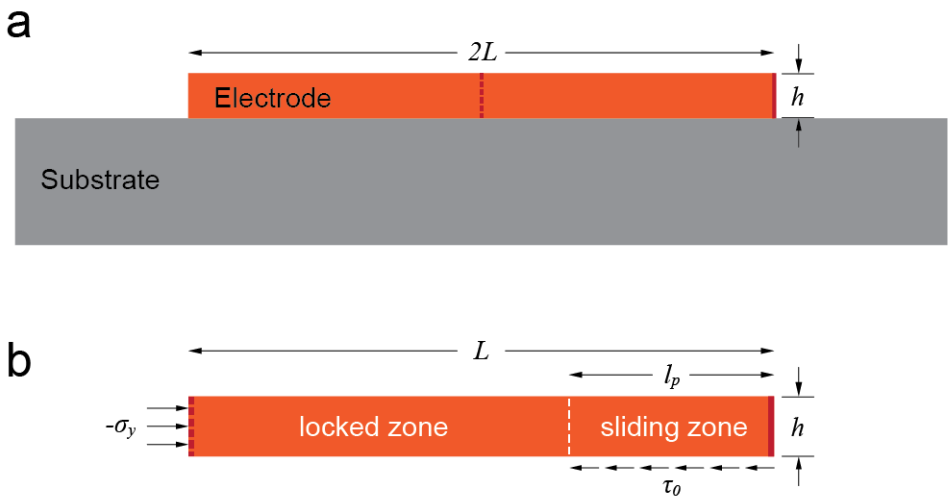

Figure A.1. (a) Schematic of a plane stress island electrode adhering and sliding on a rigid substrate. (b) Free-body diagram for the right half of the island during lithiation.

If the island size is below this critical length scale ($L < l_p$), the entire island would undergo purely elastic deformation during cycling, while if $L > l_p$, plastic deformation would take place in the locked zone. The interfacial shear stress is equal to τ_0 in the sliding zone and zero in the locked zone. The film stress in the sliding zone varies linearly from zero at the lateral surface of the island to $-\sigma_y$ at the boundary between the locked and sliding zones, and it equals to $-\sigma_y$ throughout the locked zone. Equation (A.2) indicates that l_p is a function of Li concentration c if

any one of the three system parameters σ_y, h, or τ_0 depends on c. During delithiation, the locked zone is under stress σ_y as the island shrinks and the interfacial shear stress in the sliding zone changes direction compared to that shown in Fig. A.1b.

Consider a concentration dependent interfacial sliding strength τ_0 which is equal to τ_0^u at the unlithiated state and τ_0^f at the fully-lithiated state. For convenience of analysis and without loss of generality, we assume that τ_0^u is greater than τ_0^f, and τ_0 is a function of the normalized Li concentration c as follows,

$$\tau_0 = \tau_0^u - \Delta\tau_0 c, \tag{A.3}$$

where $\Delta\tau_0 = \tau_0^u - \tau_0^f$.

The length of the sliding zone at concentration c is thus given by,

$$l_p = \frac{\sigma_y h}{\tau_0^u - \Delta\tau_0 c}. \tag{A.4}$$

The net change in length of the island during a full cycle (excluding the first cycle) can be calculated as,

$$\Delta L = \int_0^L \left(\Delta\varepsilon^e + \Delta\varepsilon^p + \Delta\varepsilon^c\right)\mathrm{d}x, \tag{A.5}$$

where $\Delta\varepsilon^e$, $\Delta\varepsilon^p$, and $\Delta\varepsilon^c$ are the change in the in-plane elastic strain, plastic strain, and compositional strain, respectively.

To rule out ratcheting induced by the thickness change of the island, only a horizontal compositional strain parallel to the interface of

$$\Delta\varepsilon^c = \beta\Delta c \tag{A.6}$$

is applied to the island electrode, and we assume that the thickness change induced by local plastic deformation is negligible.

No horizontal deformation occurs in the locked zone as the electrode material yields and the compositional strain is accommodated by plastic strain (i.e., $\Delta\varepsilon^e = 0$, $\Delta\varepsilon^p = -\Delta\varepsilon^c$), while the material in the sliding zone undergoes elastic deformation (i.e., $\Delta\varepsilon^p = 0$). Figure A.2 shows the normalized elastic strain in the right half of the island during a full cycle (excluding the first cycle) predicted by the analytical model (solid line in Fig. A.2), which agrees well with that of finite element simulations (square dots in Fig. A.2). It can be seen that the length of the sliding zone varies with Li concentration due to the concentration dependent interfacial sliding strength.

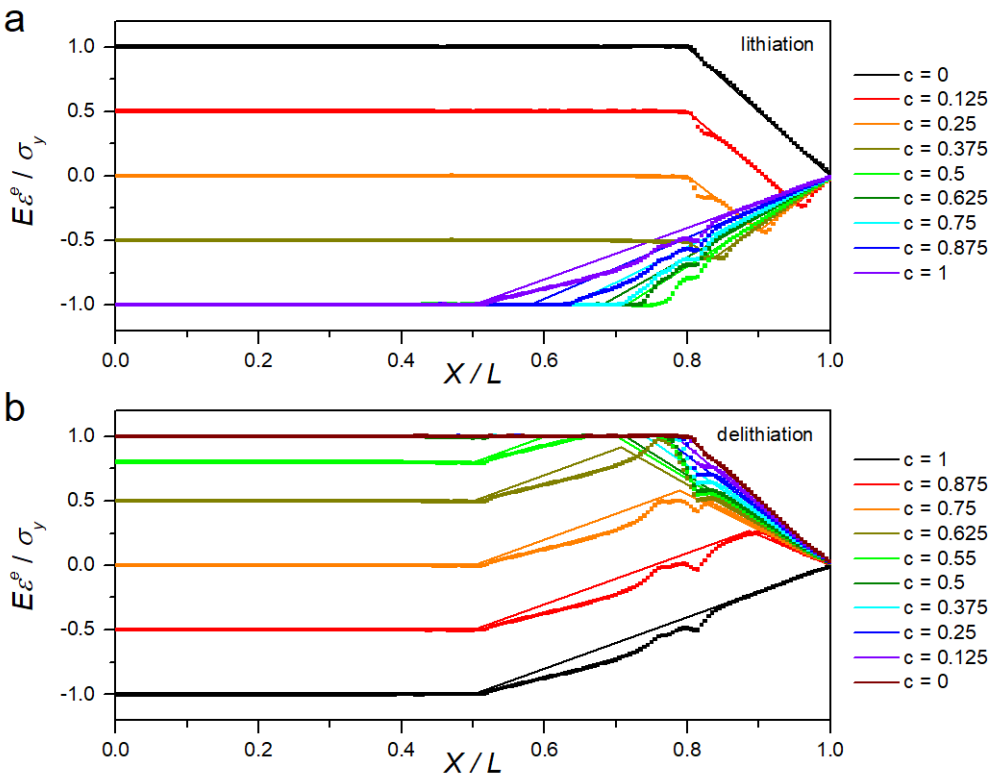

Figure A.2. Normalized elastic strain in half of the island electrode with concentration dependent interfacial sliding strength at different Li concentrations during (a) a lithiation half cycle and (b) a delithiation half cycle. The x-axis represents the normalized length coordinate of the film in the reference configuration. The results

from the theoretical model (solid lines) and those from finite element simulations (square dots) are consistent.

We identify several critical concentrations at which the deformation mode of the island changes. Figure A.3 shows the distribution of the elastic strain in the right half of the island at these critical Li concentrations:

1) During lithiation, the region at a distance of l_p^u from the edge of the island starts to expand at $c = \hat{c}$;
2) During lithiation, the center island yields at $c = c^e$;
3) During delithiation, the entire island undergoes elastic deformation until the region at a distance of $\tilde{l}_p$ from the edge yields at $c = \tilde{c}$.

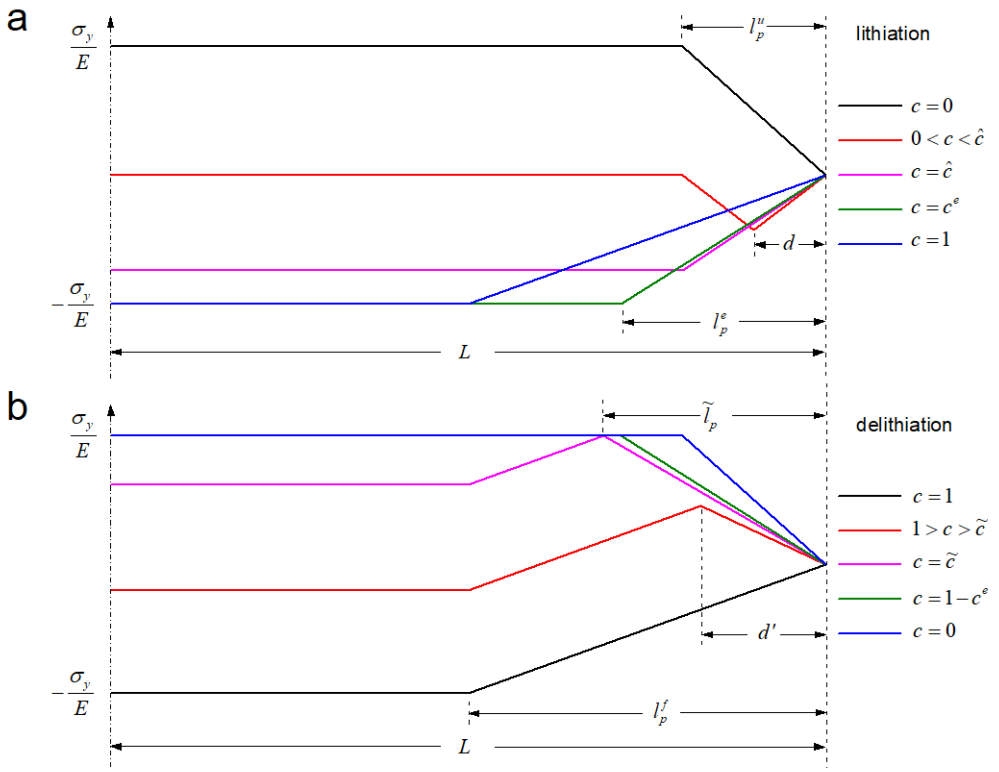

Figure A.3. Elastic strain in half of the island with concentration dependent interfacial

sliding strength at critical concentrations during (a) a lithiation half cycle and (b) a delithiation half cycle.

These critical concentrations divide the cycle into several stages. The change in half-length of the island during each stage between the critical concentrations is derived as follows:

(i) Elastic stage during lithiation ($0 < c < c^e$)

The critical concentrations can be obtained as,

$$\hat{c} = \frac{2}{E\beta/\sigma_y + \Delta\tau_0/\tau_0^u}, \quad c^e = \frac{2\sigma_y}{E\beta}. \tag{A.7a,b}$$

The length of the sliding zone at the unlithiated state is given by

$$l_p^u = \frac{\sigma_y h}{\tau_0^u}. \tag{A.8}$$

During $0 < c < \hat{c}$, the expanding region of the island (see Fig. A.3) is of length

$$d = \frac{1}{2}\left[l_p^u - \left(\frac{\sigma_y}{E} - \beta c \right) \frac{Eh}{\tau_0^u - \Delta\tau_0 c} \right]. \tag{A.9}$$

Equation (A.5) in conjunction with the elastic strain profile shown in Fig. A.3 gives the change in half-length of the island as,

$$\Delta L_{\mathrm{li}}^e(c) = \begin{cases} \dfrac{1}{2}\beta c\left(l_p^u + 2d\right) - \dfrac{\sigma_y}{E} d - \dfrac{\tau_0^u - \Delta\tau_0 c}{Eh} d^2, & 0 < c < \hat{c}, \\ \dfrac{h}{2E}\left[\dfrac{\sigma_y^2}{\tau_0^u} + \dfrac{\left(E\beta c - \sigma_y\right)^2}{\tau_0^u - \Delta\tau_0 c} \right], & \hat{c} < c < c^e. \end{cases} \tag{A.10}$$

(ii) Plastic stage during lithiation ($c^e < c < 1$)

The sliding zone lengths at c^e and c are given by,

$$l_p^e = \frac{\sigma_y h}{\tau_0^u - \Delta\tau_0 c^e}, \quad l_p = \frac{\sigma_y h}{\tau_0^u - \Delta\tau_0 c}. \tag{A.11a,b}$$

According to Eq. (A.5),

$$\begin{aligned}
&\Delta L_{\mathrm{li}}^{p}(c) \\
&= \int_{0}^{l_p^e} \left\{ \beta\left(c - c^e\right) + \frac{\sigma_y}{E}\left(\frac{1}{l_p^e} - \frac{1}{l_p}\right)\tilde{x} \right\} \mathrm{d}\tilde{x} + \int_{l_p^e}^{l_p} \left\{ \beta\left[c - \frac{\tau_0^u - \sigma_y h/\tilde{x}}{\Delta\tau_0} \right] + \frac{\sigma_y}{E}\left(1 - \frac{\tilde{x}}{l_p}\right) \right\} \mathrm{d}\tilde{x} \\
&= \beta\left[\left(c - c^e\right) l_p^e + \left(c - \frac{\tau_0^u}{\Delta\tau_0} \right)\left(l_p - l_p^e\right) + \frac{\sigma_y h}{\Delta\tau_0} \ln\frac{l_p}{l_p^e} \right] + \frac{\sigma_y}{2E}\left(l_p - l_p^e\right), \quad c^e < c < 1.
\end{aligned} \tag{A.12}$$

The net change in half-length of the island during a lithiation half cycle is thus obtained as,

$$\Delta L_{\mathrm{li}} = \Delta L_{\mathrm{li}}^{e}(c^e) + \Delta L_{\mathrm{li}}^{p}(1). \tag{A.13}$$

(iii) Elastic stage during delithiation ($1 > c > \tilde{c}$)

The change in half length of the island takes the form,

$$\Delta L_{\mathrm{de}}^{e}(c) = -\frac{Eh\beta^2(1-c)^2}{2(\tau_0^f + \tau_0^u - \Delta\tau_0 c)}, \quad 1 > c > \tilde{c}. \tag{A.14}$$

The strain profile in Fig. A.3 shows that $\tilde{c}$ satisfies the following equation,

$$\beta(1-\tilde{c}) - \frac{\tau_0^f}{E}\frac{\tilde{l}_p}{h} = \frac{\sigma_y}{E}, \tag{A.15}$$

where,

$$\tilde{l}_p = \frac{\sigma_y h}{\tau_0^u - \Delta\tau_0\tilde{c}}. \tag{A.16}$$

The solution to Eq. (A.15) takes the form,

$$\tilde{c} = \frac{1}{2}\left[\left(1 + \frac{\tau_0^u}{\Delta\tau_0} - \frac{\sigma_y}{E\beta}\right) - \sqrt{\left(1 + \frac{\tau_0^u}{\Delta\tau_0} - \frac{\sigma_y}{E\beta}\right)^2 - 4\left(\frac{\tau_0^u}{\Delta\tau_0} - \frac{\sigma_y\left(\tau_0^u + \tau_0^f\right)}{E\beta\Delta\tau_0}\right)} \right]. \tag{A.17}$$

It can be seen that the ratio of the elastic stage in a lithiation half cycle is different from that in a delithiation half cycle (i.e., $c^e \neq 1 - \tilde{c}$).

(iv) Plastic stage during delithiation ($\tilde{c} > c > 0$)

Similar to part (ii), Eq. (A.5) can be expressed as,

$$\begin{aligned}
&\Delta L_{\mathrm{de}}^{p}(c) \\
&= \int_{0}^{l_p} \left\{ \beta(c-\tilde{c}) + \frac{\sigma_y}{E}\left(\frac{1}{l_p} - \frac{1}{\tilde{l}_p}\right)\tilde{x} \right\} \mathrm{d}\tilde{x} + \int_{l_p}^{\tilde{l}_p} \left\{ \beta\left[\frac{\tau_0^u - \sigma_y h/\tilde{x}}{\Delta\tau_0} - \tilde{c} \right] + \frac{\sigma_y}{E}\left(1 - \frac{\tilde{x}}{\tilde{l}_p}\right) \right\} \mathrm{d}\tilde{x} \\
&= -\beta\left[(\tilde{c}-c) l_p + \left(\tilde{c} - \frac{\tau_0^u}{\Delta\tau_0} \right)\left(\tilde{l}_p - l_p\right) + \frac{\sigma_y h}{\Delta\tau_0} \ln\frac{\tilde{l}_p}{l_p} \right] + \frac{\sigma_y}{2E}\left(\tilde{l}_p - l_p\right), \quad \tilde{c} > c > 0.
\end{aligned} \tag{A.18}$$

The net change in half-length of the island during a delithiation half cycle is obtained as,

$$\Delta L_{\mathrm{de}} = \Delta L_{\mathrm{de}}^{e}(\tilde{c}) + \Delta L_{\mathrm{de}}^{p}(0). \tag{A.19}$$

The net change in half-length of the island during a full cycle, which is referred to as “ratcheting rate”, is thus given by

$$\Delta L / \Delta N = \Delta L_{\mathrm{li}} + \Delta L_{\mathrm{de}}. \tag{A.20}$$

The ratcheting rate can be normalized and shown to be only a function of the critical concentration c^e and interfacial sliding strengths,

$$\Delta\bar{L} / \Delta N = \frac{\Delta L / \Delta N}{\max\{|\Delta L_{\mathrm{li}}|, |\Delta L_{\mathrm{de}}|\}} = f(c^e, \tau_0^u, \tau_0^f). \tag{A.21}$$

The theoretical predictions are in good agreement with results from finite element simulations, as shown in Fig. A.4. Even though we assume that τ_0^u is greater than τ_0^f in the analysis above, the model can predict the change in half length of the island with τ_0^u less than τ_0^f by exchanging the orders and signs of ΔL_{li} and ΔL_{de}. For example, by comparing Figs. A.4b and A.4c, we can see that ΔL_{li} and ΔL_{de} satisfies the following relationship with $\tau_0^{hi} = 130\,\mathrm{MPa}$ and $\tau_0^{lo} = 10\,\mathrm{MPa}$,

$$\Delta L_{\mathrm{li}}(\tau_0^u = \tau_0^{lo}, \tau_0^f = \tau_0^{hi}) = -\Delta L_{\mathrm{de}}(\tau_0^u = \tau_0^{hi}, \tau_0^f = \tau_0^{lo}),$$
$$\Delta L_{\mathrm{de}}(\tau_0^u = \tau_0^{lo}, \tau_0^f = \tau_0^{hi}) = -\Delta L_{\mathrm{li}}(\tau_0^u = \tau_0^{hi}, \tau_0^f = \tau_0^{lo}). \quad \text{(A.22a,b)}$$

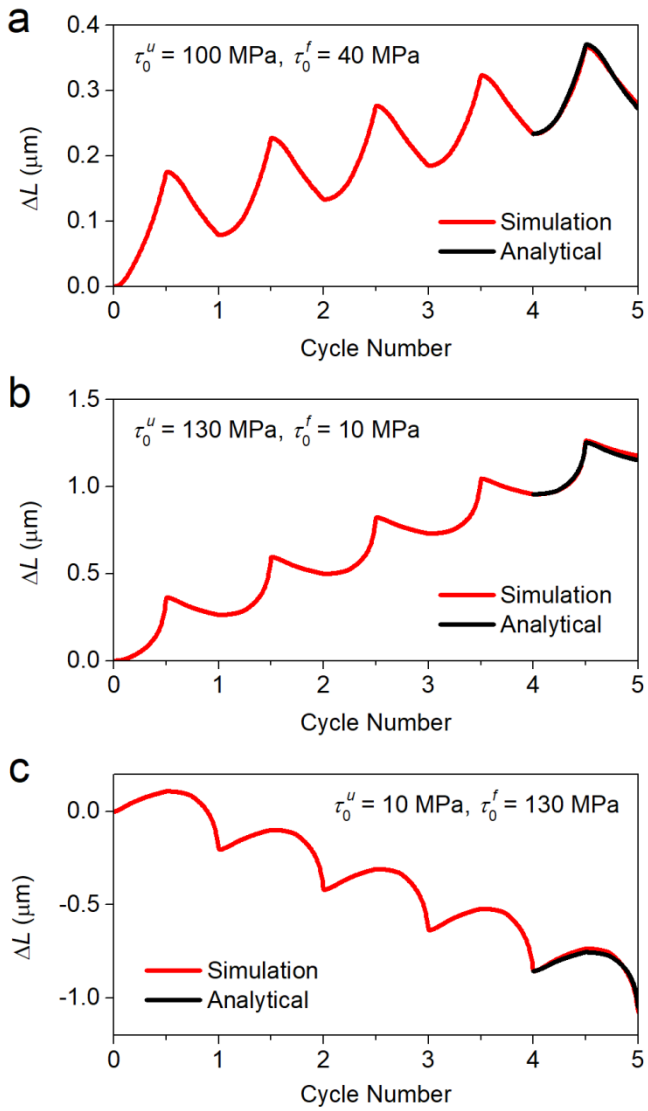

Figure A.4. Half-length changes of plane stress island electrodes with concentration dependent interfacial sliding strengths of (a) $\tau_0^u = 100\,\mathrm{MPa}$ and $\tau_0^f = 40\,\mathrm{MPa}$; (b) $\tau_0^u = 130\,\mathrm{MPa}$ and $\tau_0^f = 10\,\mathrm{MPa}$; (c) $\tau_0^u = 10\,\mathrm{MPa}$ and $\tau_0^f = 130\,\mathrm{MPa}$. The thickness, Young's modulus and yield stress of the electrode are set to 100 nm, 40 GPa and 1 GPa, respectively.

Appendix B. Supplementary material